 CMES, vol.93, no.1, pp.17-45, 2013

Construction of Operator-Orthogonal Wavelet-Based Elements for Adaptive Analysis of Thin Plate Bending Problems

Y.M. Wang[1,2], **Q. Wu**[1]

Abstract: A new kind of operator-orthogonal wavelet-based element is constructed based on the lifting scheme for adaptive analysis of thin plate bending problems. The operators of rectangular and skew thin plate bending problems and the sufficient condition for the operator-orthogonality of multilevel stiffness matrix are derived in the multiresolution finite element space. A new type of operator-orthogonal wavelets for thin plate bending problems is custom designed with high vanishing moments to be orthogonal with the scaling functions with respect to the operators of the problems, which ensures the independent solution of the problems in each scale. An adaptive operator-orthogonal wavelet method is proposed to approximate the exact solution of engineering problems by directly adding wavelets into the local domains until the relative error estimation satisfies the accuracy requirement. Numerical examples demonstrate that the operator-orthogonal method is an accurate and efficient method for bending analysis of thin plate.

Keywords: operator-orthogonal wavelet; thin plate; multiresolution analysis; lifting scheme.

1 Introduction

The wavelets have received an increased attention in the last decades in various engineering disciplines, including signal processing, processing of images, pattern recognition, diagnosing disturbances, mathematical modeling, etc. The generality of their applicability stands directly on the attractive properties, such as periodicity, orthogonality and linear independency [Chui, (1992); Daubechies (1992)]. Current wavelet-based numerical algorithms can be roughly classified as wavelet

[1] School of Automation, Xi'an University of Posts and Telecommunications,Xi'an 710121, People's Republic of China.

[2] State Key Laboratory of Acoustics, Institute of Acoustics, Chinese Academy of Sciences, Beijing 100190, China.

Galerkin [Amaratunga and Williams (1994); Mehraeen and Chen (2006)], wavelet finite element [Chen and Yang (2004); Xiang (2007, 2012)], and wavelet collocation methods [Bertoluzza and Naldi, (1996); Vasilyev (1995), Libre (2008)], etc. The wavelet implementation in the finite element analysis, named as wavelet finite element method, has attracted many researchers in the field of numerical computation [Dahlke (1997); Cohen (2003); Amaratunga (1994); Dahmen (2001); Sandeep (2011); Ho (2011); Xiang (2009); Lepik (2005)] and structural analysis[Chen (2004, 2006, 2010); Diaz (2009); He (2012); Mitra (2005); Li, Dong and Chen (2010,2012); Li and Zhang (2009); Yang (2013)]. Generally, the wavelet finite elements are constructed by adopting the shape functions to be expressed in a form of a product of wavelet functions and wavelet coefficients [Ko, Kurdila and Pilant (1995); Mallat (1999)]. A distinguished feature of wavelet finite element method is that it combines the versatility of the conventional finite element method with the accuracy of wavelet functions approximation and various in basis functions for engineering problems. Diaz constructed Daubechies wavelet finite elements for beam and plate structures and obtained higher computational accuracy than traditional finite element analysis [Diaz, Martin and Vampa (2009)]. Zhou presented a modified Daubechies wavelet approximation for deflections of beams and square thin plates with both homogeneous and non-homogeneous boundary conditions based on the modified approximations and Hamilton's principle [Zhou and Zhou (2008)]. Pahlavan proposed spectral formulation of finite element methods using Daubechies compactly-supported wavelets for elastic wave propagation simulation [Pahlavan (2013)].

Since Daubechies wavelet has no explicit expressions, traditional numerical integrals such as Gauss integral cannot provide desirable precision for the computation of stiffness matrix [Chen (2004)]. There are various wavelet basis functions with explicit expressions adopted for the construction of wavelet-based elements, such as B-spline wavelets, triangle Hermite wavelet, etc. Xiang presented wavelet-based beam and plate elements using B-spline wavelets on the interval for the bending and vibration analysis of typical structures such as beam, thin plate, etc [Xiang and Liang (2011); Xiang, Chen and He (2008); Xiang, Chen and He (2007)]. Han proposed a wavelet-based stochastic finite element method for the bending analysis of thin plates, which combines the wavelet-based finite element method with Monte Carlo method [Han, Ren and Huang (2007)]. Zupan proposed spatial triangle Hermite wavelet beam element formulation to solve spatial bending and torsion structure [Zupan, Zupan and Saje (2009)]. Because traditional wavelets are constructed by the dilation and translation of mother wavelet functions, the characteristics of wavelet bases are unable to be changed before solving engineering problems, which results in strong coupling and slow convergence rate in the multiscale computation of structural analysis.

The emergence of second generation wavelet theory [Sweldens (1997); Sweldens (1996)] has overcome the shortcomings of traditional wavelet-based method. Second generation wavelet is no longer dependent on the telescopic and translation transform, but prediction coefficients and update coefficients to construct wavelet bases flexibly with desired properties, such as compact support, symmetry, high-order vanishing moments. Thus, it provides a great deal of flexibility, and it can be designed according to the properties of the given problem. The second-generation wavelet has gradually being applied to the field of structural analysis. Vasilyev et al. established second-generation wavelet collocation method to solve elliptic and evolution equations over general geometries, such as high-dimensional, spherical domains, etc [Vasilyev (2000, 2003, 2005)]. Wang developed a multiscale lifting algorithm of second-generation wavelet-based finite element method for solving partial differential equations employing the selection of appropriate prediction and update coefficients according to the analyzed problems [Wang, Chen and He (2012)]. Behera presented the multilevel adaptive second generation wavelet collocation method for solving non-divergent barotropic vorticity equation over spherical geodesic grid [Behera (2013)].

In recent years, the generalization of the lifting scheme provides a simple way of constructing biorthogonal wavelet basis functions according to the solution requirements, such as high vanishing moments, high approximation order, symmetry, compact support, etc [Davis (1999); Shui (2004)]. The customization of second generation wavelets in the multiresolution finite element space over general geometries with the objective of developing scale-decoupling algorithms is discussed by Amaratunga, Castrillon, He, etc [Amaratunga and Sudarshan (2006); Castrillón-Candàs and Amaratunga (2003); Sudarshan (2006); He, Chen and Xiang (2007)]. Amaratunga presented a framework for the construction of operator-customized wavelets from general finite element interpolation functions, which are scale-orthogonal to the scaling functions at each level with respect to an elliptic partial differential operator [Amaratunga and Sudarshan (2006)].Castrillon used spatially adaptive lifting wavelets to represent integral operator defined on the three-dimensional geometry, which leads to highly sparse stiffness matrix and less computational time [Castrillón-Candàs and Amaratunga (2003)]. D'Heedene constructed decoupling lifting wavelets for arbitrary order Lagrange finite element basis functions on unstructured grid [D'Heedene, Amaratunga and Castrillón-Candás (2005)]. Sudarshan et al. have described a multiresolution modelling with operator-customized wavelets and demonstrated a combined approach for goal-oriented error estimation and adaptivity, where operator-customized wavelets can be constructed from general finite element interpolation functions based on lifting scheme or Gram–Schmidt orthogonalization [Sudarshan (2006)]. He proposed a new wavelet construction method by designing a suitable prediction operator and update operator according to the requirements of structural analysis [He, Chen and Xiang (2007)]. Quraishi developed a second generation wavelet-based finite element method for solving elliptic PDEs on two dimensional triangulations using customized operator dependent wavelets [Quraishi and Sandeep (2011)]. However, the present wavelets are seldom constructed with user-defined properties especially for multiscale computation of structural problems, such as the operator-orthogonality corresponding to the inner products between scaling functions and wavelets [Wang, Chen and He (2010)].

In this paper, a general construction method of operator-orthogonal wavelet-based elements based on the lifting scheme is presented for adaptive analysis of bending problems of thin plate. An outline of the paper is as follows. Section 2 introduces the multiresolution finite element space. Section 3 discusses the construction of operator-orthogonal wavelet for thin plate analysis according to the operators of the thin plate bending problems. Section 4 presents adaptive scheme for operator-orthogonal wavelet method based on the two-level error estimation. Section 5 demonstrates the numerical performance of the adaptive operator-orthogonal wavelet method and conclusions are drawn in Section 6.

2 Multiresolution finite element space

2.1 Multiresolution analysis

The second generation version of multiresolution analysis (MRA) is an important property in the multilevel approximation of engineering problems. [Sweldens (1997); Sweldens (1996)]. A multiresolution analysis R of L_2 is a sequence of closed subspaces $R = \{V_j \subset L_2 | j \in J \subset Z\}$, such that

1. $V_j \subset V_{j+1}$,

2. $\bigcup_{j\in J} V_j$is dense inL_2,

3. for each$j \in J$, V_j has a Riesz basis given by scaling functions $\left\{\phi_{j,k} | k \in K(j)\right\}$,

where j is the level of resolution, J is an integer index set associated with resolution levels, $K(j)$ is some index set associated with scaling functions of level j, V_j denotes approximation spaces of level j. For each V_j, there exists a complement of V_j in V_{j+1}, namely as W_j. Let the spaces W_j be spanned by wavelets, $\psi_{j,m}(x)$ for every $m \in M(j)$, $M(j) = K(j+1) \backslash K(j)$, where $M(j)$ is the difference set of $K(j+1)$ and $K(j)$. Furthermore, let $l \in K(j+1)$ be the index at level$j+1$.

2.2 Hermite MRA

As stated in Reference [Bathe (1996)], it is possible to construct a valid multiresolution analysis of V provided the interpolating functions are complete and compatible. Based on this premise, the scaling functions of multiresolution finite element space V_j can be chosen as the finite element interpolating functions and the wavelets are the detail interpolating polynomials in the wavelet space W_j. A multiresolution decomposition of a finite element space at different levels of resolution is spatial hierarchy:

$$V_j = W_{j-1} \oplus V_{j-1} = W_{j-1} \oplus W_{j-2} \oplus \cdots \oplus W_0 \oplus V_0 \tag{1}$$

Since the finite element spaces are nested, the relation between scaling function $\phi_{j,k}$ and wavelet $\psi_{j,m}$ at level j and $j+1$satisfies

$$\phi_{j,k} = \sum_l h_{j,k,l} \phi_{j+1,l}, \tag{2}$$

$$\psi_{j,m} = \sum_l g_{j,m,l} \phi_{j+1,l}, \tag{3}$$

where $h_{j,k,l}$ and $g_{j,m,l}$ are referred to as low-pass and high-pass filters, respectively. A multiresolution analysis allows the approximation of finite energy functions, $u(x) \in L_2(\mathbf{R})$, by a sequence of spaces V_j. $u_j(x)$ can be decomposed into its projection on a coarse approximation space V_0 along with the projections at multiple levels of wavelet spaces

$$u_j(x) = u_{j-1}(x) + d_{j-1}(x) = u_0(x) + \sum_{i=0}^{j-1} d_i(x) = \sum_l u_{0,l} \phi_{0,l} + \sum_{i=0}^{j-1} \sum_m r_{i,m} \psi_{i,m} \tag{4}$$

where $u_j(x)$ and $d_j(x)$ are the projections of the function $u(x)$ in the space V_j and W_j. $u_{0,l}$ and $r_{j,m}$ are the projection coefficients of $u(x)$ in the space V_j and W_j respectively. Eq.(4) means that the function $u(x)$ can be approximated with the projection $u_j(x)$ in V_j and the projection eventually captures all the details of the initial function $u(x)$ as scale j gets larger (i.e. $j \to \infty$), such as

$$\lim_{j \to \infty} \left\| u(x) - u_j(x) \right\| = 0 \tag{5}$$

The larger the scale the lesser the approximating error, so the details will eventually become arbitrarily small, such as

$$\lim_{j \to \infty} d_j(x) = 0 \tag{6}$$

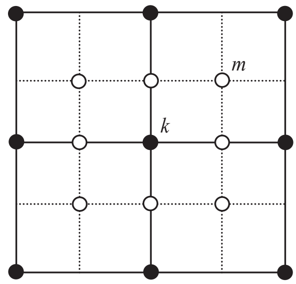

Figure 1: Refinement relation of bicubic Hermite functions

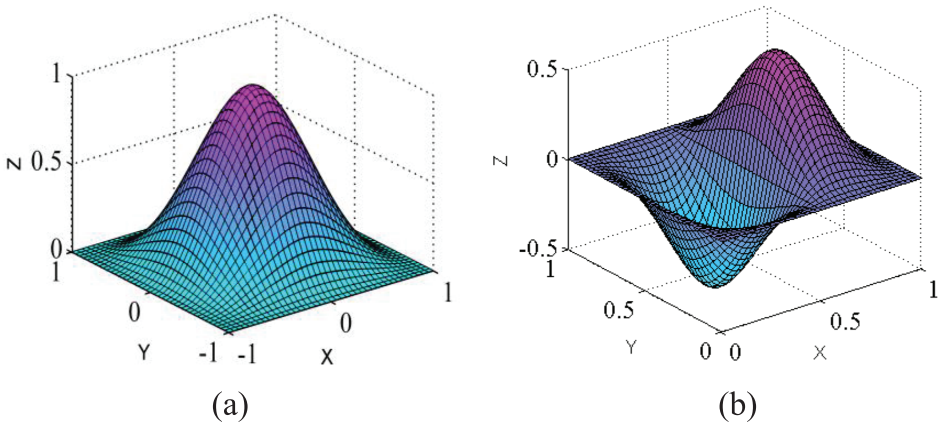

Figure 2: Bicubic Hermite scaling function and wavelet (a) scaling function (b) wavelet

Two-dimensional bicubic Hermite interpolation functions satisfy [Li and Yan (2002); Chien and Shih (2009); Wang (2002)]

$$\left[\phi_{j,k}\right] = G_{j,l}\left[\phi_{j+1,l}\right] \tag{7}$$

where

$$\left[\phi_{j,k}\right] = \left[\begin{array}{cccc} \phi_{j,k}^{(0,0)} & \phi_{j,k}^{(1,0)} & \phi_{j,k}^{(0,1)} & \phi_{j,k}^{(1,1)} \end{array}\right]^T \tag{8}$$

and the nodal degrees of freedom for $\phi_{j,k}^{(0,0)}$, $\phi_{j,k}^{(1,0)}$ and $\phi_{j,k}^{(1,1)}$ are the function value, the first partial derivatives and the cross derivative. The coefficicent matrix $G_{j,l}$ in Eq.(7) is determined by the nodal values of scaling functions on the two adjacent scale. Fig.1 shows the refinement relation of bicubic Hermite interpolation functions, where the black points denote the scaling functions, the hollow points denote the wavelet functions, the central black points denote scaling functions on the scale j and $j+1$. Fig.2 shows bicubic Hermite scaling functions and wavelets.

3 Operator-orthogonal wavelets for thin plate

3.1 The operators of thin plate

In this section, two kinds of operator-orthogonal wavelets are constructed by the lifting scheme according to the operators of thin plate bending problems in the multiresolution finite element space.

3.1.1 Rectangular thin plate

Fig.3 shows the solving domain ω of a rectangular thin plate, the side length l_x and l_y, respectively.

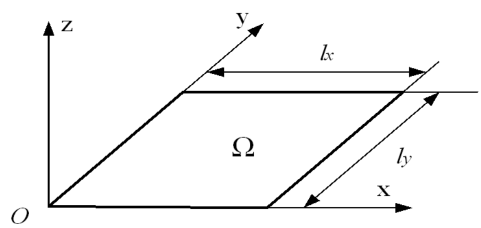

Figure 3: Solving domain of rectangular thin plate

The physical equation of thin plate bending problems is

$$\frac{\partial^2 M_x}{\partial x^2}+2\frac{\partial^2 M_{xy}}{\partial x\partial y}+\frac{\partial^2 M_y}{\partial x^2}+q=0 \tag{9}$$

According to Kirchoff plate theory, the generalized function of potential energy for a thin plate is

$$\prod\nolimits_p=\frac{1}{2}\iint\limits_{\Omega}\boldsymbol{\kappa}^{\mathrm{T}}\boldsymbol{D}\boldsymbol{\kappa}\mathrm{dxdy}-\iint\limits_{\Omega}wq\mathrm{dxdy} \tag{10}$$

where w is the displacement of the thin plate, q is uniform load, $\boldsymbol{\kappa}$ is generalized strain,

$$\boldsymbol{\kappa}=\left\{-\frac{\partial^2 w}{\partial x^2}\;-\frac{\partial^2 w}{\partial y^2}\;-2\frac{\partial^2 w}{\partial x\partial y}\right\}^{\mathrm{T}} \tag{11}$$

$\boldsymbol{D}$ is the elastic matrix in the form

$$\boldsymbol{D} = D_0 \begin{bmatrix} 1 & \mu & 0 \\ \mu & 1 & 0 \\ 0 & 0 & (1-\mu)/2 \end{bmatrix} \tag{12}$$

where $D_0 = \frac{Et^3}{12(1-\mu^2)}$ is the bending stiffness. μ is Poisson's ratio, E is Young's modulus, and t is the thickness. Applying the principle of minimum of total potential energy, $\delta\Pi_p = 0$, we obtain multiscale system of equations for thin plate in terms of Hermite scaling functions and wavelets at level $j+1$:

$$\overline{\mathbf{K}}_{j+1}\overline{u}_{j+1} = \overline{\mathbf{P}}_{j+1} \tag{13}$$

where the stiffness matrix of thin plate on the scale $j(j \geq 0, j \in Z)$ can be denoted as

$$\overline{\mathbf{K}}_{j+1} = \begin{bmatrix} \mathbf{K}_j(\phi_{j,k}, \phi_{j,k'}) & \mathbf{K}_j(\phi_{j,k}, \psi_{j,m}) \\ \mathbf{K}_j(\psi_{j,m}, \phi_{j,k}) & \mathbf{K}_j(\psi_{j,m}, \psi_{j,m'}) \end{bmatrix} \tag{14}$$

where the individual entries in $\mathbf{K}_{j+1}$ are given as

$$\mathbf{K}_j(\phi_{j,k}, \phi_{j,k'}) = a(\phi_{j,k}, \phi_{j,k'}) \quad \text{(nodal finite element matrix at level } j\text{)}, \tag{15}$$

$$\mathbf{K}_j(\phi_{j,k}, \psi_{j,m}) = a(\phi_{j,k}, \psi_{j,m}) \quad \text{(interaction matrix at level } j\text{)}, \tag{16}$$

$$\mathbf{K}_j(\psi_{j,m}, \phi_{j,k}) = a(\psi_{j,m}, \phi_{j,k}) = \mathbf{K}_j(\phi_{j,k}, \psi_{j,m}), \tag{17}$$

$$\mathbf{K}_j(\psi_{j,m}, \psi_{j,m'}) = a(\psi_{j,m}, \psi_{j,m'}) \quad \text{(detail matrix at level } j\text{)}. \tag{18}$$

where the node set $k' \in K(j)$, $m' \in M(j)$.

The stiffness matrix of thin plate in the multiresolution space is

$$\begin{aligned} \mathbf{K}_j(\phi_{j,k_1}, \phi_{j,k_2}) =& D_0 \iint_{\Omega^e} \left\{ \frac{\partial^2 \phi_{j,k_1}}{\partial x^2} \frac{\partial^2 \phi_{j,k_2}}{\partial x^2} + \frac{\partial^2 \phi_{j,k_1}}{\partial y^2} \frac{\partial^2 \phi_{j,k_2}}{\partial y^2} \right. \\ & \left. + 2(1-\mu) \frac{\partial^2 \phi_{j,k_1}}{\partial x \partial y} \frac{\partial^2 \phi_{j,k_2}}{\partial x \partial y} + 2\mu \frac{\partial^2 \phi_{j,k_1}}{\partial x^2} \frac{\partial^2 \phi_{j,k_2}}{\partial y^2} \right\} \mathrm{dxdy} \end{aligned} \tag{19}$$

The distributed forces $\overline{\mathbf{P}}_{j+1}$ and lump forces $\widehat{\mathbf{P}}_{j+1}$ on the scale j are

$$\overline{\mathbf{P}}_{j+1} = \iint_{\Omega^e} q(x)\phi_{j+1} dxdy \tag{20}$$

$$\widehat{\mathbf{P}}_{j+1} = \sum_{j+1} P_{j+1}\phi_{j+1} \tag{21}$$

The operator of thin plate bending problems can be derived as

$$\begin{aligned} a(\psi_{j,m},\phi_{j,k}) =& D_0 \iint_{\Omega^e} \left\{ \frac{\partial^2 \psi_{j,m}}{\partial x^2}\frac{\partial^2 \phi_{j,k}}{\partial x^2} + \frac{\partial^2 \psi_{j,m}}{\partial y^2}\frac{\partial^2 \phi_{j,k}}{\partial y^2} \right. \\ & \left. +2(1-\mu)\frac{\partial^2 \psi_{j,m}}{\partial x \partial y}\frac{\partial^2 \phi_{j,k}}{\partial x \partial y} + 2\mu \frac{\partial^2 \psi_{j,m}}{\partial x^2}\frac{\partial^2 \phi_{j,k}}{\partial y^2} \right\} \mathrm{dxdy} \end{aligned} \tag{22}$$

It is much desirable that the multilevel stiffness matrix are operator-orthogonal, which means that the details do not have any influence on the coarser solution and the engineering problems can be solved on different scales independent of each other. The sufficient condition for the operator-orthogonality of multilevel stiffness matrix is to construct new wavelets orthogonal with respect to the operators of the engineering problems in the multiresolution finite element space.

$$\mathbf{K}_j(\psi_{j,m},\phi_{j,k}) = a(\psi_{j,m},\phi_{j,k}) = 0 \tag{23}$$

According to Eqs. (2) and (3), the scaling functions and wavelet at a certain level j can be represented as a linear combination of scaling functions on the finer level $j+1$. Therefore, the operator-orthogonality in Eq. (23) at level j ensures that the operator-orthogonality at random level $\widetilde{j}(\widetilde{j} \in J)$ be satisfied [Amaratunga and Sudarshan (2006)]

$$a(\psi_{j,m},\phi_{j,k}) = \widetilde{H}_{\widetilde{j},\widetilde{k}} a(\psi_{j,m},\phi_{\widetilde{j},\widetilde{k}}) = 0 \quad (\widetilde{k} \in K(\widetilde{j})) \tag{24}$$

$$a(\psi_{j,m},\psi_{\widetilde{j},\widetilde{m}}) = \widetilde{G}_{\widetilde{j},\widetilde{k}} a(\psi_{j,m},\phi_{\widetilde{j},\widetilde{k}}) = 0 \quad (\widetilde{m} \in M(\widetilde{j})) \tag{25}$$

where $\widetilde{H}_{\widetilde{j},\widetilde{k}}$ and $\widetilde{G}_{\widetilde{j},\widetilde{k}}$ are the low-pass and high-pass filter matrices, respectively.

3.1.2 Skew thin plate

Fig.4 shows the solving domain Ω of a skew thin plate, α denotes the skew angle of thin plate.

The oblique coordinate system is constructed when the operator-orthogonal wavelet method is used to solve skew thin plate bending problems. The relationship between the oblique coordinate system xoy and the Cartesian coordinate system $\widehat{x}o\widehat{y}$ has the form

$$\begin{bmatrix} x \\ y \end{bmatrix} = \begin{bmatrix} 1 & -1/\tan\alpha \\ 0 & 1/\sin\alpha \end{bmatrix} \begin{bmatrix} \widehat{x} \\ \widehat{y} \end{bmatrix} \tag{26}$$

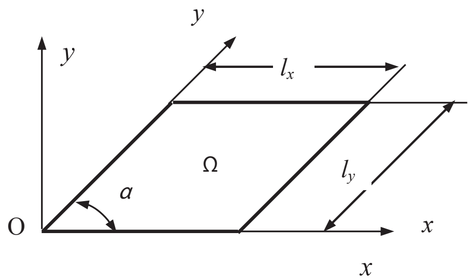

Figure 4: Solving domain Ω of skew thin plate

The generalized function of potential energy of skew thin plate in the Cartesian coordinate system can be derived as

$$\begin{aligned}\mathbf{\Pi}_p =& \frac{D_0}{2}\iint\limits_{\Omega}\{(\frac{\partial^2 w}{\partial \widehat{x}^2}+\frac{\partial^2 w}{\partial \widehat{y}^2})^2-2(1-\mu)[\frac{\partial^2 w}{\partial \widehat{x}^2}\frac{\partial^2 w}{\partial \widehat{y}^2} \\ &-(\frac{\partial^2 w}{\partial \widehat{x}\partial \widehat{y}})^2]\}d\widehat{x}d\widehat{y}-\iint\limits_{\Omega} q(\widehat{x},\widehat{y})wd\widehat{x}d\widehat{y}\end{aligned} \tag{27}$$

According to the principle of minimum of total potential energy, $\delta\mathbf{\Pi}_p = 0$, the multilevel system of equations for skew thin plate on the scale $j+1$ can be derived as

$$\overline{\mathbf{K}}_{j+1}\overline{u}_{j+1} = \overline{\mathbf{P}}_{j+1} \tag{28}$$

where the distributed forces $\overline{\mathrm{P}}_{j+1}$ and lump forces $\widetilde{\mathrm{P}}_{j+1}$ on the scale $j+1$ are

$$\overline{\mathbf{P}}_{j+1} = \sin\alpha \iint_{\Omega^e} q(x)\phi_{j+1}dxdy \tag{29}$$

$$\widetilde{\mathbf{P}}_{j+1} = \sin\alpha \sum_{j+1} P_{j+1}\phi_{j+1} \tag{30}$$

where P_{j+1} is concentrated loads. The stiffness matrix of skew thin plate in the multiresolution space is

$$
\begin{aligned}
\mathbf{K}_j(\phi_{j,k_1},\phi_{j,k_2}) =& D_0 \iint_{\Omega^e} \left\{ \frac{\partial^2\phi_{j,k_1}}{\partial x^2}\frac{\partial^2\phi_{j,k_2}}{\partial x^2} + \frac{\partial^2\phi_{j,k_1}}{\partial y^2}\frac{\partial^2\phi_{j,k_2}}{\partial y^2} \right. \\
& - 4\cos\alpha(\frac{\partial^2\phi_{j,k_1}}{\partial x^2}\frac{\partial^2\phi_{j,k_2}}{\partial x\partial y} + \frac{\partial^2\phi_{j,k_1}}{\partial y^2}\frac{\partial^2\phi_{j,k_2}}{\partial x\partial y}) \\
& + 2(1-\mu\sin^2\alpha+\cos^2\alpha)\frac{\partial^2\phi_{j,k_1}}{\partial x\partial y}\frac{\partial^2\phi_{j,k_2}}{\partial x\partial y} \\
& \left. + 2(\mu\sin^2\alpha+\cos^2\alpha)\frac{\partial^2\phi_{j,k_1}}{\partial x^2}\frac{\partial^2\phi_{j,k_2}}{\partial y^2} \right\} \mathrm{dxdy}
\end{aligned}
\tag{31}
$$

The operator of skew thin plate problems is

$$
\begin{aligned}
a(\psi_{j,m},\phi_{j,k}) =& D_0 \iint_{\Omega^e} \left\{ \frac{\partial^2\psi_{j,m}}{\partial x^2}\frac{\partial^2\phi_{j,k}}{\partial x^2} + \frac{\partial^2\psi_{j,m}}{\partial y^2}\frac{\partial^2\phi_{j,k}}{\partial y^2} \right. \\
& - 4\cos\alpha(\frac{\partial^2\psi_{j,m}}{\partial x^2}\frac{\partial^2\phi_{j,k}}{\partial x\partial y} + \frac{\partial^2\psi_{j,m}}{\partial y^2}\frac{\partial^2\phi_{j,k}}{\partial x\partial y}) \\
& + 2(1-\mu\sin^2\alpha+\cos^2\alpha)\frac{\partial^2\psi_{j,m}}{\partial x\partial y}\frac{\partial^2\phi_{j,k}}{\partial x\partial y} \\
& \left. + 2(\mu\sin^2\alpha+\cos^2\alpha)\frac{\partial^2\psi_{j,m}}{\partial x^2}\frac{\partial^2\phi_{j,k}}{\partial y^2} \right\} \mathrm{dxdy}
\end{aligned}
\tag{32}
$$

3.2 Construction of operator-orthogonal wavelets

The lifting scheme proposed by Sweldens is a flexible method for the construction of various new wavelet bases with the desired characteristics. For any multiresolution space, a compactly supported lifting wavelet is built by adding adjacent scaling functions $\phi_{j,k}$ into the original wavelets $\psi^{old}_{j,m}$, which is usually selected by the scaling function $\phi_{j+1,m}$ [Sweldens (1997); Sweldens (1996)]:

$$\psi_{j,m} = \psi^{old}_{j,m} - \sum_k s_{j,k,m}\phi_{j,k} = \phi_{j+1,m} - \sum_k s_{j,k,m}\phi_{j,k} \tag{33}$$

where $s_{j,k,m}$ are the lifting coefficients. Substituting Eqs. (2) and (3) into Eq. (33), we obtain

$$\psi_{j,m} = \sum_l g_{j,m,l}\phi_{j+1,l} - \sum_k s_{j,k,m}(\sum_l h_{j,k,l}\phi_{j+1,l}) = H_{j+1,l}\phi_{j+1,l} \tag{34}$$

In order to meet the operator-orthogonality in the multiscale computation of engineering problems, the lifting coefficient matrix $H_{j+1,l}$ can be computed using techniques for computing a basis for the null space of the interaction matrix $a(\phi_{j,k*}$,

$\phi_{j+1,l})$ as

$$a\left(\phi_{j,k*},\psi_{j,m}\right)=H_{j+1,l}a\left(\phi_{j,k*},\phi_{j+1,l}\right)=0 \tag{35}$$

where $\phi_{j,k*}$ are all scaling functions on the domains Ω_j, k^* are the nodes of scaling functions on Ω_j. For general engineering problems, the operator-orthogonal wavelet bases can be constructed with $n+1$ vanishing moments with respect to the variables $x$and y

$$\begin{bmatrix} a\left(\phi_{j,k*},\psi_{j,m}\right) \\ a\left(x^n y^n,\psi_{j,m}\right) \end{bmatrix}=H_{j+1,l}\begin{bmatrix} a\left(\phi_{j,k*},\phi_{j+1,l}\right) \\ a\left(x^n y^n,\phi_{j+1,l}\right) \end{bmatrix}=0 \tag{36}$$

The number of the solution of Eq. (36) determines the number of lifted wavelets. The principle of constructing lifted wavelets is to choose proper lifted coefficients from Eq. (36) such that the lifted wavelets are compactly support and the lifting coefficient vectors are linearly independent. Fig.5 shows bicubic Hermite operator-orthogonal wavelets constructed form bicubic Hermite scaling functions with one vanishing moments according to Eq.(36).

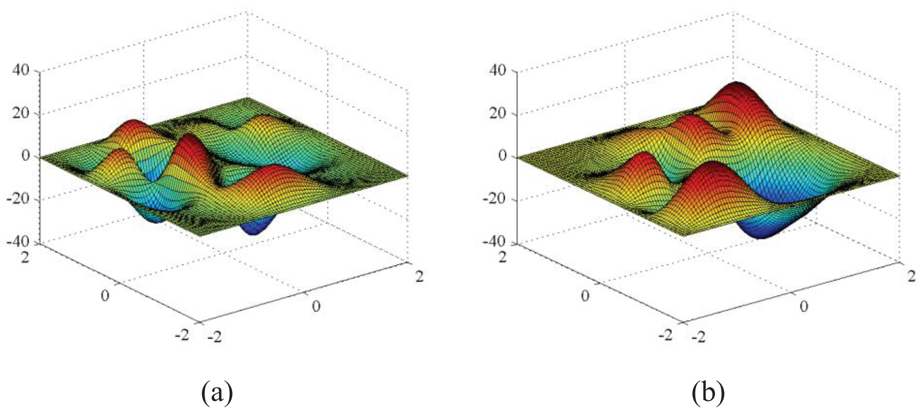

Figure 5: Bicubic Hermite operator-orthogonal wavelets with one vanishing moments

4 Adaptive operator-orthogonal wavelet-based method

4.1 Error analysis

The error estimator of the operator-orthogonal wavelet solution is the key parameter to test the accuracy of operator-orthogonal wavelet method. A two-level error estimator ε_j (also called global error estimator) of operator-orthogonal wavelet method is chosen to be the uniform norm of the difference e_j between the operator-orthogonal wavelet solution $\bar{u}_{j+1}$ and $\bar{u}_j$ at two levels $j+1$ and j respectively in the form

$$\varepsilon_j = \left\|e_j\right\|_\infty = \max\left|\bar{u}_{j+1} - \bar{u}_j\right| \tag{37}$$

The dimensionless form of global error estimator η_j (also called global relative error estimator) on the domain Ω_j for the operator-orthogonal wavelet method can be defined as

$$\eta_j = \frac{\max\left|\bar{u}_{j+1} - \bar{u}_j\right|}{\max\left|\bar{u}_{j+1}\right|} \tag{38}$$

The local error estimator λ_j^r of an operator-orthogonal wavelet solution in any local domain Ω_j^r ($r = 1, 2, \cdots$ is the number of local domains) is

$$\lambda_j^r = \left|\bar{u}_{j+1}^r - \bar{u}_j^r\right| \tag{39}$$

According to the refinement relation in Eq. (4), the operator-orthogonal wavelet solution can be obtained by using all the operator-orthogonal wavelets on the domain Ω_j^r. As the scale becomes larger, it can be ensured that the error estimator becomes small to satisfy a random threshold value.

4.2 Adaptive operator-orthogonal wavelet algorithm

Reference [Wang, Chen and He (2010)] proposed a multiscale operator-orthogonal wavelet method, also called the multiscale refinement, which gradually approximates the exact solution by adding operator-orthogonal wavelets into global solving domain. In order to solve engineering problems efficiently, an adaptive operator-orthogonal wavelet algorithm, also called adaptive refinement, is proposed. The engineering problems can be solved using the proposed method by adding operator-orthogonal wavelets into local domains with error estimators higher than the given threshold. The adaptive operator-orthogonal wavelet algorithm is given below:

Given error toleranceτ, the threshold value for wavelet refinement $\vartheta (0 < \vartheta \leq 1)$, given initial domain Ω_0 at the scale $j = 0$ and the local domains Ω_j^r, the engineering problems can be solved according to the following steps:

(1) Calculate initial operator-orthogonal wavelet solution u in the solving domain Ω_0;

(2) Calculate global relative error estimate η_j, if $\eta_j < \tau$, stop the calculation and output the result;

(3) Calculate all the local error estimate λ_j^r in the local domains Ω_j^r and determine the maximum local error estimates $\lambda_j^{\max} = \max(\lambda_j^r)$;

(4) Generate all local domains that satisfy $\lambda_j^r \geq \vartheta \lambda_j^{\max}$, and save a list of local domains $\widetilde{\Omega}_j^r$;

(5) Add detail matrices $\mathrm{K}_j(\psi_{j,m}, \psi_{j,m'})$ into the multi-scale stiffness matrices $\overline{\mathrm{K}}_{j+1}$ in the local domains $\widetilde{\Omega}_j^r$ and let $j = j+1$;

(6) Solve the multiscale operator-orthogonal wavelet equations and update the operator-orthogonal wavelet solutions and solving domains Ω_j^r, go to (2).

The key for the proposed numerical method is the procedures (3) and (4), in which the local domains are selected according to the local error estimate and the threshold value condition. The operator-orthogonality of multilevel stiffness and mass matrices ensures the incremental computation of eigenvalue solution by the adaptive operator-orthogonal wavelet algorithm. Since the steering parameter ϑ is chosen randomly, an increasing number of operator-orthogonal wavelets can be added into the local domains and the convergence rate of the solution can be adjusted to users' computational requirements.

5 Numerical examples

In this section, numerical experiments are presented to demonstrate the efficiency and flexibility of adaptive operator-orthogonal wavelet algorithm. As common structural problems [Rao and Chaudhary (1988); Morley (1963); Timoshenko and Woinowsky-Krieger (1959)], rectangular and skew thin plates are solved by multiscale [He, Chen and Xiang (2007); Wang, Chen and He (2010)] and adaptive operator-orthogonal wavelet method, respectively. In the numerical examples, the threshold values for multiscale and adaptive operator-orthogonal wavelet algorithms are set to be equivalent for the comparison of the accuracy and efficiency. We choose a random threshold value of 0.5 in the numerical examples.

Example 1 Bending analysis of square thin plate simply supported on all four sides on all four sides, the parameters are given as: plate length L, thickness t, singular load $q_0 = qe^{-100*[(x/L-0.5)^2+(y/L-0.5)^2]}$, elastic modulus E, Poisson's ratioμ.

The bicubic Hermite operator-orthogonal wavelets shown in Fig.6 are constructed according to the operator-orthogonality in Eq.(18). Fig.7 shows the relative error of the displacements of square thin plate using multiscale and adaptive operator-orthogonal wavelet solution (Abbreviated as multiscale and adaptive wavelet algorithms) with increasing number of levels and degrees of freedoms. It can be seen that the multi-scale and adaptive operator-orthogonal wavelet method has almost the same convergence rate, but the adaptive operator-orthogonal wavelet method approximates the exact solution with fewer degrees of freedom. Fig.8 shows deformation of square plate simply supported on all four sides. The contour plots

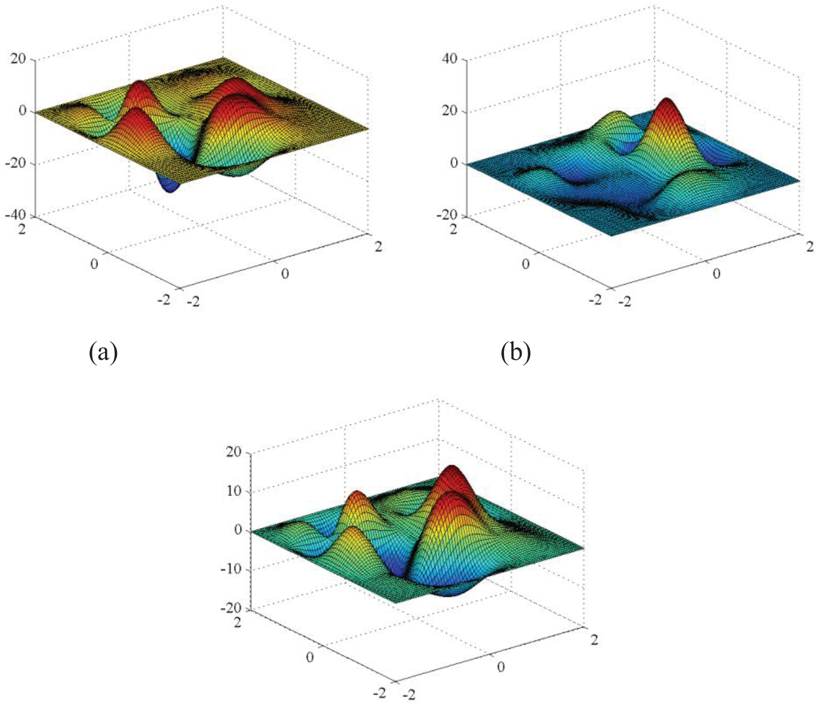

(a) (b) (c)

Figure 6: Bicubic Hermite wavelets with (a) two (b) two (c) three vanishing moments

of the deformed plate along y direction are shown in Fig.9, the bottom dotted line is the deformation of middle line along y direction and the upper line is the simply supported side. Table 1 illustrates the convergence rate of the displacements by multiscale and adaptive operator-orthogonal wavelet solution with respect to number of levels and degrees of freedoms, respectively. The comparison of the central displacement, central moment and torque moment of the corner points obtained by multiscale, adaptive operator-orthogonal wavelet solution and traditional Shell63 element solution (commercial software ANSYS) with 100×100 meshes is shown in Tables 2. It can be seen that the operator-orthogonal wavelet solutions are match well with those of ANSYS and the degrees of freedom (DOFs) of adaptive operator-orthogonal wavelet method are much less than the other methods.

Example 2 Bending analysis of skew thin plate subjected to uniform load, the parameters are given as: plate length L, thickness t, uniform load q, elastic modulus

Table 1: Operator-orthogonal wavelet solution for the displacements of square plate simply supported on all four sides

Space		Multiscale			Adaptive	
	DOFs	ε_j (10^{-2}) $w\ 100D_0/qL^4$	$\eta_j(\%)$	DOFs	ε_j (10^{-2}) $w\ 100D_0/qL^4$	$\eta_j(\%)$
V0(j=0)	36	——	——	36	——	——
W0(j=0)	64	0.90303	20.4754	32	0.92721	21.1063
W1(j=1)	224	0.52636	14.2061	40	0.56845	16.2794
W2(j=2)	832	0.15164	4.6232	156	0.16651	5.1581
W3(j=3)	3200	0.08288	2.5763	582	0.08770	2.7215

Table 2: Central displacements and moments of square plate simply supported on all four sides

Method	$w\ 100D_0/qL^4$	$M_x 10/qL^2$	$M_y 10/qL^2$	$M_{xy} 10/qL^2$	DOFs
ANSYS	0.033339	0.061465	0.061465	0.019865	61206
Multiscale operator-orthogonal wavelet	0.033308	0.060239	0.060239	0.019322	66564
Error(%)	0.0930	1.9946	1.9946	2.7335	
Adaptive operator-orthogonal wavelet	0.033296	0.060173	0.060173	0.019208	5682
Error(%)	0.1290	2.1020	2.1020	3.3073	

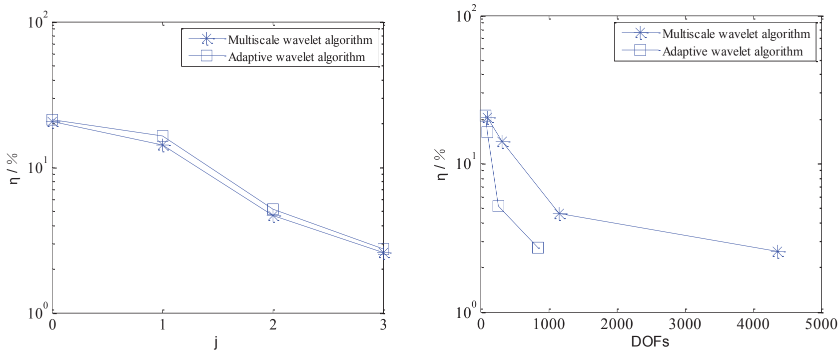

(a) (b)

Figure 7: Convergence rate of square plate simply supported on all four sides with (a) number of levels (b) degrees of freedom

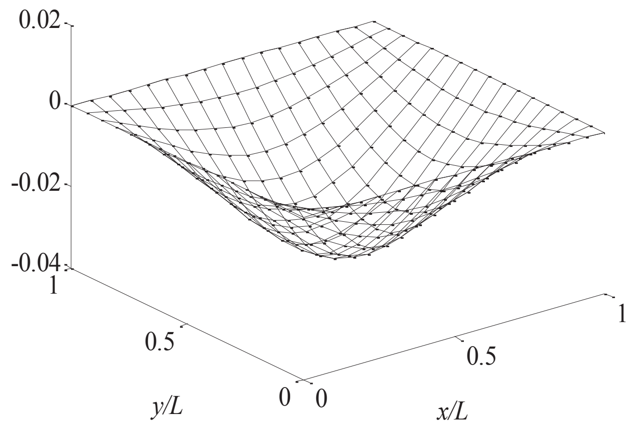

Figure 8: Deformed plate

E, Poisson's ratio μ, bevel angle α.

Fig.10 shows bicubic Hermite operator-orthogonal wavelets satisfying the operator-orthogonality in Eq.(25). Fig.11 illustrates the relative error of the displacements of skew plate using multiscale and adaptive operator-orthogonal wavelet solution with increasing number of levels and degrees of freedoms for the skew plate, respectively. Fig.12 shows deformation of clamped skew plate, which is subjected to uniform load. The contour plots of the deformed plate along y direction are shown in Fig.13, the deformation of middle line along y direction is shown as dotted.

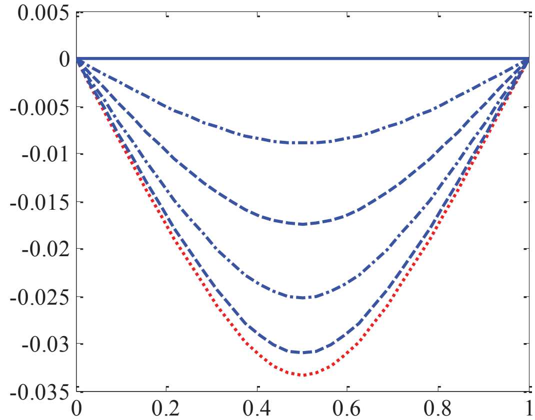

Figure 9: Contour plots along y direction

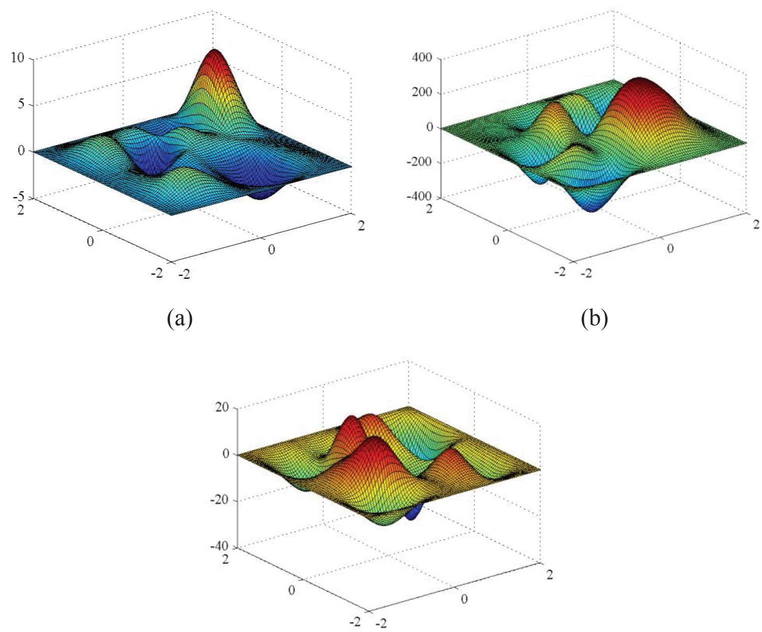

(a)

(b)

(c)

Figure 10: Bicubic operator-orthogonal Hermite wavelets with (a) two (b) three (c) three vanishing moments

Table 3 illustrates the convergence rate of the displacements of clamped skew plate under α=45° using the multi-scale and adaptive operator-orthogonal wavelet method, respectively. The comparison of the central displacement, central moment and torque moment of the corner points obtained by multiscale, adaptive operator-orthogonal wavelet solution and ANSYS Shell63 element solution with 100×100 meshes is shown in Tables 4. It can be seen that numerical solution of the problems using three methods has the same convergence rate, but adaptive operator-orthogonal wavelet method approximates the analytic solution with fewer degrees of freedom. Table 5 illustrates the adaptive operator-orthogonal wavelet solution on the scale j=3 and the solution in Reference [Rao, 1988; Morley, 1963] of skew plate under different oblique angle. Table 6 shows the adaptive operator-orthogonal wavelet solution on the scale j=4 of central displacement and moment and those of the other FEM (Zienkiewicz, 1988) for the skew plate under skew angle α=60°. Both the displacement and moment results indicate that the adaptive operator-orthogonal wavelet method has higher accuracy and less meshes. It can be seen that the analyzed problem is computed with much fewer degrees of freedom although the adaptive solution is close to the solution obtained by multi-scale refinement.

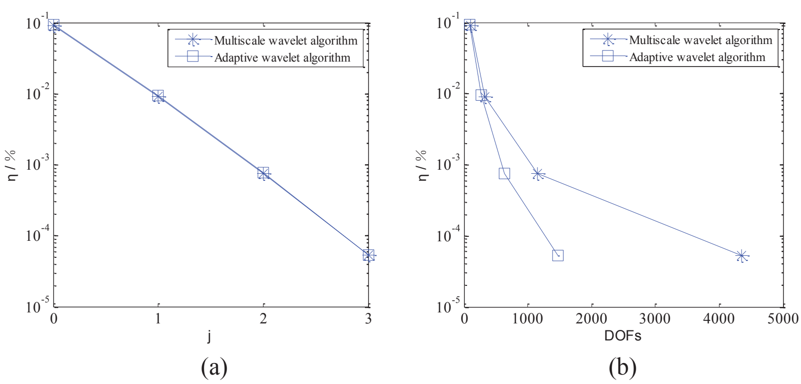

Figure 11: Convergence rate of skew plate under angle α=45° with (a) number of levels (b) degrees of freedom

Example 3 Bending analysis of skew thin plate simply supported on two parallel sides, fixed on the other two sides, the parameters are given as: plate length L, thickness t, load $q_0 = q\sin(\frac{\pi x}{L})\sin(\frac{\pi y}{L})$, elastic modulus E, Poisson's ratio μ, bevel angle α.

The construction method of operator-orthogonal wavelets is the same as those in Fig.10. Fig.14 shows the convergence rate of the displacements of skew plate using

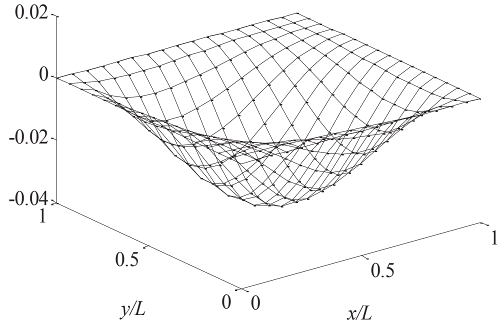

Figure 12: Deformed plate

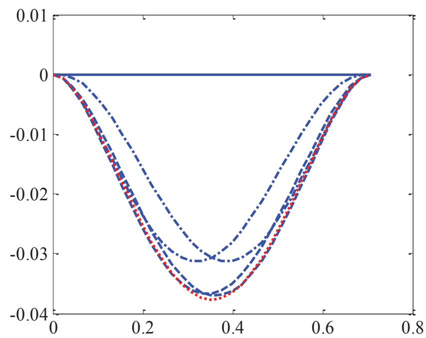

Figure 13: Contour plots along y direction

Table 3: Operator-orthogonal wavelet solution for the displacements of clamped skew plate under α=45°

Space		Multiscale			Adaptive	
	DOFs	ε_j (10^{-2}) w $100D_0/qL^4$	$\eta_j(\%)$	DOFs	ε_j (10^{-2}) w $100D_0/qL^4$	$\eta_j(\%)$
V0(j=0)	36	——	——	36	——	——
W0(j=0)	64	0.32409	9.0685	56	0.33117	9.2813
W1(j=1)	224	0.03304	0.9086	184	0.03428	0.9501
W2(j=2)	832	0.00279	0.0754	366	0.00280	0.0759
W3(j=3)	3200	0.00020	0.0053	836	0.00020	0.0053

multiscale and adaptive operator-orthogonal wavelet solution with increasing number of levels and degrees of freedoms. Fig.15 shows deformation of skew thin plate

Table 4: Central displacements and moments of clamped skew plate

Method	$w\ 100D_0/qL^4$	$M_x 10/qL^2$	$M_y 10/qL^2$	$M_{xy} 10/qL^2$	DOFs
ANSYS	0.037699	0.098505	0.13401	0.034579	61206
Multiscale operator-orthogonal wavelet	0.037721	0.098987	0.13464	0.034127	66564
Error(%)	0.0584	0.4893	0.4701	1.3072	
Adaptive operator-orthogonal wavelet	0.037706	0.098853	0.13418	0.033759	6042
Error(%)	0.0186	0.3533	0.1269	2.3714	

Table 5: Central displacement $w \times 1000 \times D_0/qL^4$of skew plates for simply supported and clamped boundary conditions at all four sides (j=3)

Skew angle α	Simply supported skew plate subjected to uniform load of intensity q			Clamped skew plate subjected to uniform load of intensity q		
	Adative operator-orthogonal wavelet	(Rao, 1988)	(Morley, 1963)	Adative operator-orthogonal wavelet	(Rao, 1988)	(Morley, 1963)
90°	4.0624	4.06	4.06	1.2719	1.27	1.26
85°	4.0143	4.01	4.01	1.2511	–	–
80°	3.8739	3.87	3.87	1.2031	1.20	1.20
75°	3.6317	3.64	–	1.1229	–	–
70°	3.3052	–	–	1.0160	1.02	1.02
60°	2.5525	2.56	2.56	0.7629	0.771	0.769
55°	2.1331	2.14		0.6306	–	–
50°	1.7116	1.72	1.72	0.4980	0.503	0.500
45°	1.3108	1.32	–	0.3771	–	–
40°	0.9437	0.958	0.958	0.2652	0.269	0.270
30°	0.3894	0.406	0.408	0.1043	0.108	–

simply supported on two parallel sides, fixed on the other two sides. The contour plots of the deformed plate along y direction are shown in Fig.16, the bottom dotted line is the maximum deformation along y direction and the upper line is the simply supported side. Table 7 illustrates the convergence rate of the displacements of skew plate under skew angle α=30° by the multi-scale and adaptive operator-orthogonal wavelet method, respectively. The comparison of maximum displacements and moments by multiscale and adaptive operator-orthogonal wavelet-based

Table 6: Comparison of adaptive operator-orthogonal wavelet results (j=4) of central displacement and moment of the skew plate under α=60° with those of traditional FEM (Zienkiewicz, 1988)

(a) Central displacement $w \times 100 \times D_0/qL^4$							
Mesh	DKQ	ACQ	LSL-Q12	MITC4	MiSP4	MMiSP4	DSQ
8×8	0.7876	0.7920	0.7918	0.7610	0.7781	0.7604	0.7840
12×12	0.7909	0.7927	0.7927	0.7785	–	–	–
16×16	0.7920	0.7930	–	–	0.7894	0.7832	0.7871
Exact	0.7945						
Adaptive operator-orthogonal wavelet	0.7914						
(b) Central moment $M_y \times 10/qL^2$							
Mesh	DKQ	ACQ	LSL-Q12	MITC4	MiSP4	MMiSP4	DSQ
8×8	0.9605	0.9990	0.9777	0.9090	0.9423	0.9052	0.9609
12×12	0.9602	0.9777	0.9680	0.9370	–	–	–
16×16	0.9601	0.9700	–	–	0.9567	0.9466	0.9602
Exact	0.9589						
Adaptive operator-orthogonal wavelet	0.9622						

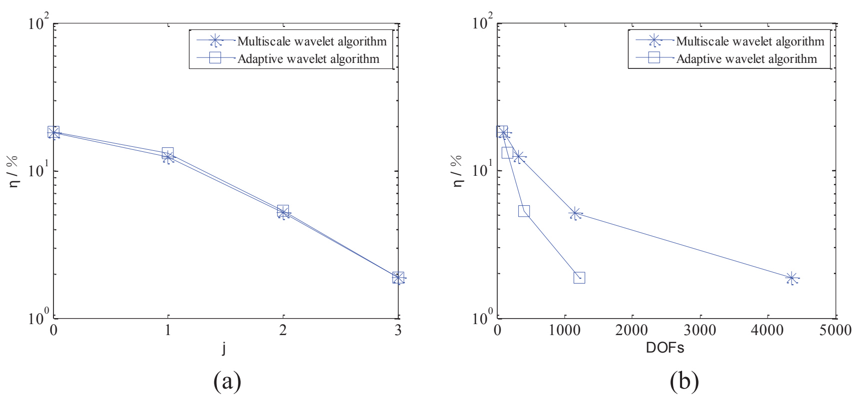

Figure 14: Convergence rate of skew plate under oblique angle α=60° with (a) number of levels (b) degrees of freedom

solution with Shell63 element solution with 100×100 meshes is given in Table 8. The adaptive operator-orthogonal wavelet method shows its advantage over the other two other methods in solving skew plate bending problems with less computational cost.

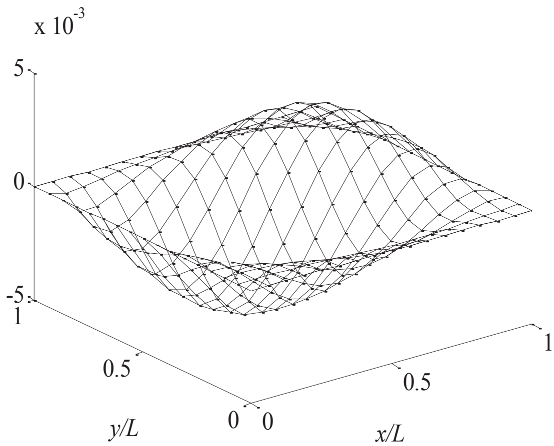

Figure 15: Deformed plate

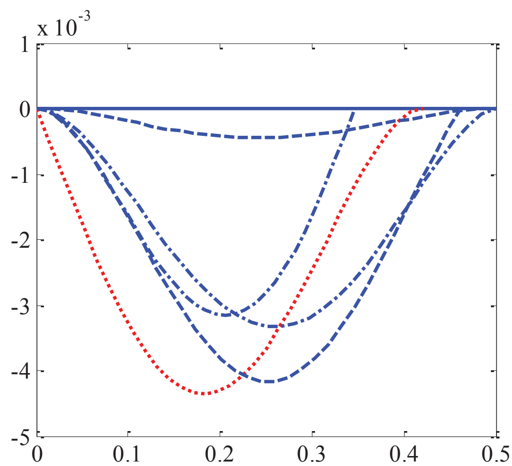

Figure 16: Contour plots along y direction

6 Conclusions

Based on the derivation of the operator of thin plate bending problems, the lifting scheme is used to construct operator-orthogonal wavelets to meet operator-orthogonality of thin plate problems. The numerical examples demonstrate that the operator-orthogonal wavelet-based method realizes independent and accurate solution of thin plate problems in each scale, which is a useful tool to deal with high performance computation in structural analysis. Compared with the traditional fi-

Table 7: Operator-orthogonal wavelet solution for the displacements of skew plate under oblique angle α=30°

Space		Multiscale			Adaptive	
	DOFs	ε_j (10^{-3}) $w\ 100D_0/qL^4$	$\eta_j(\%)$	DOFs	ε_j (10^{-3}) $w\ 100D_0/qL^4$	$\eta_j(\%)$
V0(j=0)	36	–	–	36	–	–
W0(j=0)	64	0.75039	18.0295	40	0.76390	18.3671
W1(j=1)	224	0.52387	12.3858	76	0.55323	13.0952
W2(j=2)	832	0.22428	5.1605	248	0.23156	5.3342
W3(j=3)	3200	0.08148	1.8665	820	0.08137	1.8659

Table 8: Maximum displacements and moments of skew plate

Method	$w\ 100D_0/qL^4$	$M_x 10/qL^2$	$M_y 10/qL^2$	$M_{xy} 10/qL^2$	DOFs
ANSYS	0.0043764	0.031042	0.057672	0.023103	61206
Multiscale operator-orthogonal wavelet	0.0043773	0.031353	0.058538	0.022591	66564
Error(%)	0.0206	1.0019	1.5016	2.2162	
Adaptive operator-orthogonal wavelet	0.0043759	0.031329	0.058405	0.022482	7216
Error(%)	0.0114	0.9246	1.2710	2.6880	

nite element method, the adaptive operator-orthogonal wavelet method uses less degrees of freedom to approximate the exact solution of engineering problems. It also shows that operator-orthogonal wavelets bases are attractive for multiscale computation. The advantage of the proposed method over traditional finite element method is that it adds the operator-orthogonal wavelets into the local domains based on two-level error estimation until the solution error satisfies the accuracy requirement. It is promising that the proposed method can be extended to three-dimensional or general structural analysis.

Acknowledgements

We would like to thank two anonymous reviewers for several important comments and suggestions that helped in improving the clarity and presentation of our original manuscript. The work in this article is supported by National Natural Science Foundation of China (No. 51205309, 61100165), Natural Science Basic Research Plan in Shaanxi Province of China (No. 2013JQ7025) and Research Fund of State

Key Laboratory of funded project for Acoustics (No. SKLA201309).

References

Amaratunga, K.; Williams, J.R.; Qian, S.; Weiss, J. (1994): Wavelet–Galerkin solutions for one-dimensional partial differentialequations. *Int. J. Numer. Meth. Eng.,* vol. 37, pp.2703–2716.

Amaratunga, K.; Sudarshan, R. (2006): Multiresolution modeling with operator-customized wavelets derived from finite elements. *Comput. Methods Appl. Mech. Engrg.,* vol.195, pp. 2509-2532.

Bathe, K.J. (1996) : *Finite Element Procedures*. Prentice-Hall: Upper Saddle River, NJ.

Behera, R.; Mehra, M. (2013): Integration of barotropic vorticity equation over spherical geodesic grid using multilevel adaptive wavelet collocation method. *Appl. Math Model*, vol37, no. 7, pp. 5215-5226

Bertoluzza, S.; Naldi, G.(1996): A wavelet collocation method for the numerical solution of partial differential equations, *Appl. Comput. Harmon. A.*, vol. 3, no.1, pp. 1–9.

Castrillón-Candàs, J.; Amaratunga, K. (2003): Spatially adapted multiwavelets and sparse representation of integral equations on general geometries. *SIAM J. Sci. Comput.,* vol. 24, no. 5, pp. 1530–1566

Chen, X.F.; He, Z.J.; Xiang J.W.; Li, B. (2006): A dynamic multiscale lifting computation method using Daubechies wavelet. *J. Comput. Appl Math*, vol. 188, no. 2, pp. 228-245.

Chen, X.F.; Xiang, J.W.; Li, B.; He, Z.J. (2010): A study of multiscale wavelet-based elements for adaptive finite element analysis. *Adv in Eng Softw*, vol. 41, no. 2, pp. 196-205.

Chen, X.F.; Yang, S.J.; Ma, J.X., He, Z.J. (2004): The construction of wavelet finite element and its application, *Finite Elem. Anal. Des.*, vol. 40, pp. 541–554.

Chien C.S.; Shih Y.T. (2009): A cubic Hermite finite element-continuation method for numerical solutions of the von Kármán equations. *Appl Math Comput*, vol. 209, no. 2, pp. 356–368

Chui, C.K. (1992): *An Introduction to Wavelets*. Academic Press, Boston.

Cohen, A. (2003) : *Numerical Analysis of Wavelet Method*, Elsevier Press, Amsterdam, Holland.

Dahlke, S.; Dahmen, W.; Hochmulth, R.; Schneider, R. (1997): Stable multiscale bases and local error estimation for elliptic problems. *Appl Numer. Math.*, vol. 23, pp. 21–47.

Dahmen, W. (2001): Wavelet methods for PDEs some recent developments. *J. Comput Appl Math*, vol. 128, no. 1–2, pp. 133–185.

Davis, G.M.; Strela, V.; Turcajova, R (1999): *Multiwavelet Construction via the lifting scheme*. In Wavelet Analysis and Multiresolution Methods, He TX (ed.). Lecture Notes in Pure and Applied Mathematics. Marcel Dekker: New York.

Daubechies, I. (1992): *Ten lectures on wavelets*. CBMS—NSF regional conference series in applied mathematics. Department of Mathematics, University of Lowell, MA. SIAM, Philadelphia.

Diaz, L.A.; Martin, M.T.; Vampa V. (2009): Daubechies wavelet beam and plate finite elements. *Finite Elem. Anal. Des*, vol. 45, no. 3, pp. 200-209.

D'Heedene, S.; Amaratunga, K.; Castrillón-Candás, J. (2005): Generalized hierarchical bases: a Wavelet–Ritz–Galerkin framework for Lagrangian FEM. *Eng. Comput.*, vol. 22, no. 1, pp. 15–37.

Han, J.G.; Ren, W.X.; Huang, Y. (2007): A wavelet-based stochastic finite element method of thin plate bending. *Appl. Math Model*, vol. 31, no. 2, pp. 181–193.

He, YM., Chen, XF., Xiang, JW., He, Z.J. (2007): Adaptive multiresolution finite element method based on second generation wavelets. *Finite Elem. Anal. Des.*, vol. 43, no. 6-7, pp. 566 – 579.

He, W.Y.; Ren, W.X. (2012): Finite element analysis of beam structures based on trigonometric wavelet. *Finite Elem. Anal. Des.*, vol.51 pp. 59–66.

Ho, S.L.; Yang, S.Y. (2001): Wavelet-Galerkin method for solving parabolic equations in finite domains. *Finite Elem. Anal. Des.*, vol. 37 no. 12, pp. 1023-1037

Ko J. Kurdila, A.J.; Pilant, M.S. (1995): A class of finite element methods based on orthonormal, compactly supported wavelets, *Comput Mech*, vol. 16, pp.235–244.

Lepik, Ü. (2005): Numerical solution of differential equations using Haar wavelets. *Math. Comput. Simulat*, vol. 68, no. 2, pp. 127-143.

Li, B.; Dong, H.B. (2012): Quantitative Identification of Multiple Cracks in a Rotor Utilizing Wavelet Finite Element Method. *CMES Comput. Model. Eng. Sci.,* vol 84, no. 3, pp. 205-228.

Li, B.; Chen, X.F.; He, Z.J. (2010): A wavelet-based error estimator and an adaptive scheme for plate bending problems. *Int J. Comp Meth-Sing.*, vol. 7, no. 2, pp. 241-259.

Li, Z.; Zhang, W.; Gong, K. (2009): Wavelet-based Inclusion Detection in Cantilever Beams. *CMC: Comput, Mater. Con*, vol. 9, no. 3, 209-228.

Li, Z.C.; Yan, N.N. (2002): New error estimates of bi-cubic Hermite finite element methods for biharmonic equations. *J. Comput. Appl. Math*, vol. 142, no. 2, pp. 251-285.

Libre, N.A.; Emdadi, A.; Kansa, E.J.; Shekarchi, M.; Rahimian, M. (2008): A fast adaptive wavelet scheme in RBF collocation for nearly singular potential PDEs. *CMES Comput. Model. Eng. Sci.,* vol.38, no.3, 263-284.

Mallat S.G. (1999): A Wavelet Tour of Signal Processing, *Academic Press*, New York.

Mehraeen, S.; Chen, J.S. (2006): Wavelet Galerkin method in multiscale homogenization of heterogeneous materials. *Int. J. Numer. Meth. Eng.*, vol. 66, pp. 381–404.

Mitra, M.; Gopalakrishnan, S. (2005): Spectrally formulated wavelet finite element for wave propagation and impact force identification in connected 1-D waveguides. *Int J Solids Struct.*, vol. 42, no. 16–17, pp. 4695–4721.

Morley, D.(1963): Skew Plates and Structures . New York: Pergamon Press.

Pahlavan, L.; Kassapoglou, C.; Gürdal, Z. (2013): Spectral formulation of finite element methods using Daubechies compactly-supported wavelets for elastic wave propagation simulation. *Wave Motion*, vol. 50, no. 3, pp. 558-578.

Quraishi, S.M.; Sandeep, K. (2011): A second generation wavelet based finite element on triangulations. *Comput. Mech*, vol. 48, no. 2, pp. 163-174.

Rao, H.; Chaudhary, V.K. (1988): Analysis of skew and triangular plates in bending. *Comput. Struct*, vol. 28, no.2, pp. 223$\sim$235.

Sandeep, K.; Gaur, S.; Dutta, D.; Kushwaha, H.S. (2011): Wavelet based schemes for linear advection–dispersion equation. *Appl. Math. Comput*, vol. 218, no.7, pp.3786–3798.

Shui, P.L.; Bao, Z. (2004): M-Band Biorthogonal Interpolating Wavelets via Lifting Scheme. *IEEE T. Signal Proces*, vol. 52, no. 9, pp. 2500-2512.

Sudarshan, R.; Amaratunga, K.; Grätsch, T. (2006): A combined approach for goal-oriented error estimation and adaptivity using operator-customized finite element wavelets. *Int. J. Numer. Meth. Eng.* vol. 66, pp. 1002–1035.

Sweldens, W. (1997): The lifting scheme: a construction of second generation wavelets. *SIAM J. Math. Anal*, vol. 29, no. 2, pp. 511–546.

Sweldens, W. (1996): The lifting scheme: a custom-design construction of biorthogonal wavelets. *Appl. Comput. Harmon. A*, vol. 3, no. 2, pp. 186–200.

Timoshenko, S.P.; Woinowsky-Krieger, S. (1959): *Theory of Plates and Shells.* 2^{nd} Edition, McGraw-Hill.

Vasilyev, O.V. (2003): Solving multi-dimensional evolution problems with localized structure using second generation wavelets. *Int. J. Comp.Fluid Dyn.*, vol. 17, no. 2, pp. 151–168.

Vasilyev, O.V,; Bowman, C. (2000): Second generation wavelet collocation method for the solution of partial differential equations. *J. Comput. Phys*, vol. 165, no.2, pp. 660–693.

Vasilyev, O.V.; Paolucci, S.; Sen, M. (1995): A multilevel wavelet collocation method for solving partial differential equations in a finite domain. *J. Comput. Phys*, vol. 120, no.1, pp. 33–47.

Vasilyev, O.V.; Kevlahan, NK-R. (2005) An adaptive multilevel wavelet collocation method for elliptic problems. *J. Comput. Phys*, vol. 206, no.2, pp. 412–431.

Wang, X.C. (2002): *The finite element methods (in Chinese)*.Tsing Hua University Press, Beijing.

Wang, Y.M.; Chen, X.F.; He, Y.M.; He, Z.J. (2010): New decoupled wavelet bases for multiresolution structural analysis. *Struct. Eng Mech*, vol. 35, no. 2, pp. 195-207.

Wang, Y.M.; Chen, X.F.; He, Z.J (2012): A second-generation wavelet-based finite element method for the solution of partial differential equations. *Appl. Math. Lett*, vol. 25, no.11, pp. 1608-1613.

Xiang, J.W.; Chen, X.F.; He, Z.J.; Zhang, Y.H. (2008): A new wavelet-based thin plate element using B-spline wavelet on the interval. *Comput. Mech*, vol. 41, no.2, pp. 243-255.

Xiang, J.W.; Chen, X.F.; He, Y.M.; He, Z.J. (2007): Static and vibration analysis of thin plates by using finite element method of B-spline wavelet on the interval. *Struct. Eng. Mech.*, vol. 25, no. 5, pp. 613-629.

Xiang, J.W.; Chen, X.F.; Li, X.K. (2009): Numerical solution of Poisson equation with wavelet bases of Hermite cubic splines on the interval. *Appl. Math. Mech.-Engl.,* vol. 30, no. 10, pp. 1325-1334.

Xiang, J.; Liang, M. (2011): Multiple damage detection method for beams based on multi-scale elements using Hermite cubic spline wavelet. *CMES Comput. Model. Eng. Sci.,* vol.73, no.3, pp.267-298.

Xiang, J.W.; Wang, Y.X.; Jiang, Z.S. et al. (2012): Numerical simulation of plane crack using hermite cubic spline wavelet. *CMES Comput. Model. Eng. Sci.,* vol. 88, no.1, pp. 1-16.

Yang, Z.B.; Chen, X.F.; Zhang, X.W.; He, Z.J. (2013): Free vibration and buckling analysis of plates using B-spline wavelet on the interval Mindlin element. *Appl. Math. Model*, vol.37, no.5, pp. 3449-3466.

Zhou, Y.H.; Zhou, J. (2008): A modified wavelet approximation of deflections for solving PDEs of beams and square thin plates. *Finite Elem. Anal. Des.*, vol. 44, no. 12-13, pp. 773-783.

Zienkiewicz, O.C.; Lefebvre, D. (1988): A robust triangular plate bending element of the Reissener-Mindlin type. *Int. J. Numer. Methods Eng.*, vol. 26 1169-1184.

Zupan, E.; Zupan, D.; Saje, M. (2009): The wavelet-based theory of spatial naturally curved and twisted linear beams. *Comput Mech*, vol. 43, no. 5, pp. 675-686.